Thesis for the Degree of Licentiate of Engineering

Optimal Near-field Antenna Apertures in Lossy Media

Aidin Razavi

CHALMERS

Department of Signals and Systems
Chalmers University of Technology

Göteborg, Sweden 2014

Optimal Near-field Antenna Apertures in Lossy Media

Aidin Razavi

Technical report number: R011/2014
ISSN 1403-266X

Department of Signals and Systems
Antenna Systems Division
Chalmers University of Technology
SE–412 96 Göteborg
Sweden
Telephone: +46 (0)31 – 772 1000
Email: aidin.razavi@chalmers.se

Typeset by the author using LaTeX.

Chalmers Reproservice
Göteborg, Sweden 2014

To my family

"You see, wire telegraph is a kind of a very, very long cat. You pull his tail in New York and his head is meowing in Los Angeles. Do you understand this? And radio operates exactly the same way: you send signals here, they receive them there. The only difference is that there is no cat."

-Albert Einstein

Abstract

Antennas are traditionally designed for far-field applications such as wireless communications, radar, etc., where the antenna systems interact with other systems and objects which are located in the far-field zone of the antennas. For this reason, the characterization of antennas in the far-field is well-defined and measurable by well-developed measurement techniques both in line-of-sight and multipath environments. However, with the recent increase in applications for near-field microwave systems such as in detection and sensing, wireless power transfer or near-field communication, there is a need for the study of design criteria of antennas tailored for near-field applications. This thesis addresses some aspects of this topic.

In order to assess the antenna's ability to transfer power to a desired target in the near-field, *penetration ability* is introduced and investigated besides the directivity which is a far-field characteristic. It can be demonstrated that these near-field and far-field characteristics are not explicitly correlated and that the penetration ability is dependent on the depth of interest in the near-field as well as the loss in the medium.

The axial pattern cannot be defined and used in lossy media since in the presence of loss, the field intensity is affected by a monotonous attenuation with distance from the antenna. The *3dB near-field beam radius* is introduced as a measure to characterize the antenna's focusing behavior in lossy media in the near-field and it is further used to find an optimal size of the uniform field apertures for the near-field detection of foreign objects in lossy media.

In the final part, array signal processing techniques are applied to the transmitting aperture field modes in order to determine the optimal aperture distribution that maximizes the power transmission through lossy media. The optimal apertures which are determined by this method are applicable in many near-field systems, such as the detection of foreign objects in lossy matters (e.g. food contamination detectors), wireless charging of batteries of human body implanted devices, and for near-field communication systems.

Keywords: near-field antennas, maximum penetration, near-field focusing,

optimal near-field aperture, near-field power transfer, array signal processing.

Preface

This thesis is in partial fulfillment for the degree of Licentiate of Engineering at Chalmers University of Technology.

The work resulting in this thesis was done between June 2011 and April 2014. It has been performed within the Antenna Systems Division, Department of Signals and Systems, at Chalmers. Professor Mats Viberg is the examiner, Associate Professor Jian Yang is the main supervisor and Assistant Professor Rob Maaskant is the co-supervisor.

The work has been supported by a grant from the Swedish Research Council (VR).

Acknowledgment

First and foremost, I wish to thank my supervisor Associate Professor Jian Yang, for the great opportunity he has given me and for his continuous support, guidance and encouragement during these years. I would also like to thank my co-supervisor Assistant Professor Rob Maaskant for the interest, attention and time he has put in my work. We have had many fruitful discussions and I look forward to our future collaboration in the coming years. Furthermore, I wish to express my gratitude to Professor Mats Viberg for examining this thesis and for his warm welcome during our first visit to Sweden which was one the encouraging factors for me to choose Chalmers over other options. I would like to express my appreciation to Professor Per-Simon Kildal for creating a great and friendly research environment in the Antenna Systems Division.

My special thanks to all former and current colleagues in the Signals and Systems department, for creating a nice and enjoyable work environment. I've been fortunate to work with all of you in such a friendly and multi-cultural place. I would like to particularly thank my dear friends Astrid, Ahmed and Carlo. We've had so many fun and enjoyable moments both in work and afterwork time. Furthermore, I wish to express my special thanks to Hasan and Oleg for being the best officemates.

I've had great time, being surrounded by so many great friends in the large Iranian community in, and around Chalmers. Ali, Ashkan, Azita, Bahram, Behrooz, Mitra, Mona, Negar, Roozbeh and Sahar. Thank you all for reminding me of home, when I'm so far from it.

I'd like to express my deepest gratitude to my parents and my sister for always being there for me, supporting and encouraging me at every step I take. Special thanks to my in-laws for their kind heart and support.

Last but not least, my most sincere gratitude to my beloved Maryam, for her lovely company in this journey. Without you I wouldn't have come this far.

Aidin

List of Publications

This thesis is based on the work contained in the following appended papers:

Paper 1

A. Razavi, and J. Yang, "Investigation of Penetration Ability of UWB Antennas in Near-field Sensing Applications", in *Proceedings of the 6th European Conference on Antennas and Propagation, EUCAP 2012*, Prague, Czech Republic, March 2012.

Paper 2

A. Razavi, J. Yang, and T. McKelvey, "Optimal Aperture Distribution of Near-Field Antennas for Maximum Signal Penetration", in *Proceedings of the 7th European Conference on Antennas and Propagation, EUCAP 2013*, Gothenburg, Sweden, April 2013.

Paper 3

A. Razavi, and J. Yang, "Optimal Size of Uniform Aperture for Near-field Penetration Through Lossy Medium", submitted to *Microwave and Optical Technology Letters.*

Paper 4

A. Razavi, R. Maaskant, J. Yang, and M. Viberg, "Maximum Aperture Power Transmission in Lossy Homogeneous Matters", submitted to *Antennas and Wireless Propagation Letters.*

Contents

Part I

Introductory Chapters

Chapter 1

Introduction

Traditionally, antennas have been designed and used for far-field applications. Over the years, many different design concepts and antennas have been developed for wireless communications, radar, telemetry and various other applications where antenna systems interact with one another and with objects that are located in the far-field zone of the antennas. This means that the characterization of antennas in the far-field, both in Line-of-sight (LOS) and multipath applications, is well-defined and can be evaluated by well-developed measurement techniques [1–3].

On the other hand, near-field microwave systems find more and more applications in recent years in areas such as detection and sensing [4–7], wireless power transfer [8], or near-field communication. In these applications, the purpose of the antenna system is to interact with the immediate surroundings which often constitutes a lossy medium. The antenna which is used in many such applications, is often one which is designed with far-field criteria and associated limitations in mind. However, as it can be demonstrated, a good antenna designed with far-field properties does not necessarily provide the optimal performance in the near-field.

With the aforementioned increase in near-field microwave applications, there is a need for systematic study and design of antennas and criteria tailored for near-field applications. However, the characterization, design criteria, and fundamental limitations of antennas in the near-field – specially when dealing with lossy materials – has not been addressed as thorough as in the far-field. This thesis addresses some of aspects of this topic.

1.1 Aim of the Thesis

The aim of this thesis is to introduce and investigate different characteristics and design criteria for antennas in near-field applications dealing with

lossy materials and to explore fundamental limitations of idealized aperture antennas in these problems. With this goal in mind, the Penetration Ability is introduced as the ratio of the received power by the supplied power when two antennas are located on two sides of a lossy medium. By investigating the penetration ability, it can be observed that most far-field characteristics of antennas are not directly applicable in the near-field.

Since the focus of the work is on characteristics and limitations of antennas, it is natural to work on ideal aperture antennas instead of on the actual realization of the antenna. By this approach it is possible to determine the optimal aperture distribution as an upper bound for what can actually be realized. The goal in the design of the antenna will be to synthesize an aperture that closely resembles the optimal one, but the possible hurdles in the design process are not of major concern in this work since they are not expected to pose a severe problem.

Two approaches are taken to deal with the problem of near-field focusing. The first approach is through the introduction of the 3dB near-field beam radius, which shows how the energy is focused along a path in front of the antenna. Although the minimization of the beam radius does not necessarily result in the maximization of the received power, it can be shown that it affects the scattering from small objects, which can be useful in many near-field sensing applications. By using the 3dB near-field beam radius definition, we can define an optimal size of the uniform field apertures in the near-field based on the electrical properties and thickness of the media surrounding the antenna.

The second approach is to directly maximize the power coupling between two antenna apertures in a lossy medium. For sensing applications, it is conjectured that maximizing the power transfer ratio leads to larger perturbations to the received signal when a foreign object is present. However, the potential applications of the power transfer ratio maximization are not limited to sensing as it can also be beneficial in the design of wireless power transfer and near-field communication systems. These approaches are discussed and examined in the following chapters, as outlined below, and can be found as appended papers as well.

1.2 Thesis Outline

The thesis is divided in two main parts. The purpose of the first part, consisting of 6 chapters, is to introduce the subject and to summarize the results of this work. Chapter 2 offers a brief review of earlier work related to near-field focusing apertures, thereby clarifying the context of the work. Chapter 3 introduces Penetration Ability as a way to characterize antennas

in near-field lossy media. In Chapter 4, the 3dB near-field beam radius is introduced as a means of characterizing the antenna's performance to focus the radiated power in the near-field, which is subsequently used to investigate the optimal size of a uniform aperture. Chapter 5 presents a method of finding the optimal aperture field distribution for maximizing the near-field power coupling between a pair of antennas, which is beneficial for both the detection of foreign objects, as well as for the optimal power transfer and near-field communication links in lossy media. Chapter 6 concludes the first part of the thesis with a brief summary of the contributions and provides an overview of future work. The second part of the thesis includes author's contributions in the form of four appended papers.

Chapter 2

Background

Earlier research on the topic of near-field focusing apertures can be summarized into two main categories as "Focused Apertures" and "Classic Infinite Apertures". These two categories are briefly reviewed in this chapter.

2.1 Focused Apertures

Since the 1950's there has been studies on so-called "Focused apertures". On a "focused aperture", a spherical phase front is employed to focus the energy of the field at a certain distance in the Fresnel zone [9, 10]. It was shown that on the focal plane, near its axis, the electric field of a focused aperture exhibits several properties of the far-field, among which that a tapered aperture distribution results in decreased sidelobe levels, increased beamwidth, and a decreased gain. In addition, it has been shown that the actual location of the maximum field intensity along the axis of the aperture is not exactly at the intended focal distance set by the aperture phase distribution. The corresponding offset is dependent on the size of the aperture and the focal distance [9]. On the other hand, it has been shown that an inverse taper gives rise to low forelobes and aftlobes[1], but also to high sidelobes and a large reduction in gain [10]. The axial pattern of focused antennas can be synthesized by using methods similar to those used for synthesizing far-field patterns, where the focal distance is controlled separately by aperture the phase distribution. The control over the axial pattern comes at the cost of a degradation in the angular or transverse pattern as an increase in the width of the main beam or an increase in the sidelobe level [11]. Successful attempts in realizing focused apertures have been made by employing large microstrip arrays or Fresnel zone plate

[1] Forelobes and aftlobes are defined as the axial lobes before and after the focal distance, respectively [10].

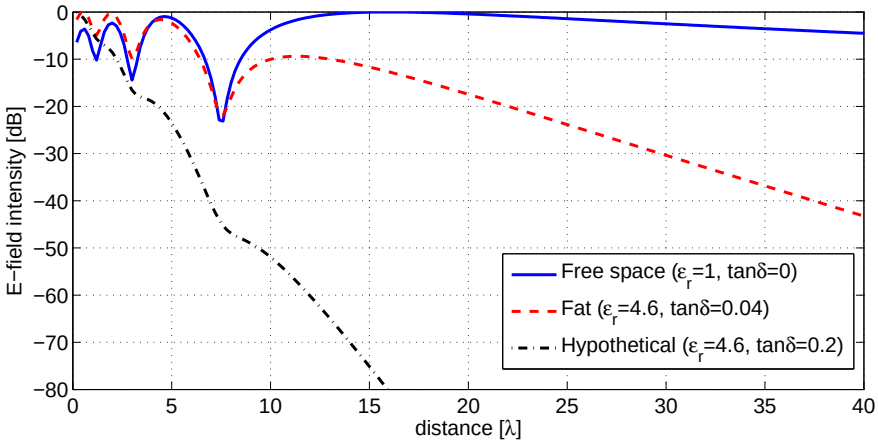

Figure 2.1: The E-field intensity on the axis for a circular uniform field aperture of radius 4λ vs. distance from the aperture in three different media.

lenses [12, 13]. However, none of the above-mentioned earlier works have taken loss in the medium into account in their investigations.

Kay [14] has investigated the near-field gain of aperture antennas in an attempt to maximize it. However, the analytical approach in [14] falls short when determining the exact optimal aperture field distribution due to its computational complexity for the time. Borgiotti [15] has used the reaction integrals in order to formulate and maximize the power transfer between two planar apertures in the near-field. However, the field distribution in the latter work can be analytically solved only in the particular case of rectangular apertures.

Fig. 2.1 shows the E-field intensity on the axis of a circular uniform aperture of radius 4λ in three media each with a different conductivity. As can be seen in Fig. 2.1, as soon as loss is introduced to the medium, the axial pattern, forelobes and aftlobes cannot be defined any longer so that new characteristics need to be defined and used. The 3dB near-field beam radius, which will be discussed in Chapter 4, is a suitable and useful parameter in this regard.

2.2 Classical Infinite Apertures

Two classical infinitely large aperture field distributions providing interesting near-field beam characteristics have been examined in the past. One of them is the Bessel aperture [16, 17] where the E-field distribution at the

distance z from the aperture plane is given by

$$\boldsymbol{E}(\rho, z) = E_0 J_0 \left(k_\rho \rho'\right) \mathrm{e}^{-jk_z z} \hat{\boldsymbol{y}} \tag{2.1}$$

where J_0 is the zero-order Bessel function of the first kind and k_z and k_ρ are the longitudinal and transverse components of the wave vector, which satisfy

$$k_z^2 + k_\rho^2 = k^2 \tag{2.2}$$

where k is the wavenumber in the medium. The main beam that is generated by a Bessel aperture field is diffraction-free, which means that its radius is constant at any distance from the aperture. However, due to the form of the Bessel function, the sidelobes form an infinite number of rings around the main beam and it can be shown that the power contained in each ring is approximately the same as that in the main beam [18]. In order to limit the power, a finite aperture size assuming a Bessel distribution (Pseudo-Bessel) is employed. The finiteness of the aperture will, in turn, result in an oscillating main beam intensity up to a certain distance z_{max}, after which the peak intensity decays [16]. Pseudo-Bessel beams can be generated by, e.g., patch antenna arrays [19], open-ended waveguide (guided modes) [20] or leaky-wave modes [21]. The radius of the main beam for a pseudo-Bessel aperture is not constant, even at distances shorter than z_{max}. In fact, the finiteness of the aperture will not only result in a decaying peak power, but also results in an oscilating beam radius in the region between the aperture and z_{max}, beyond which it widens continuously as can be seen in Fig. 2.2.

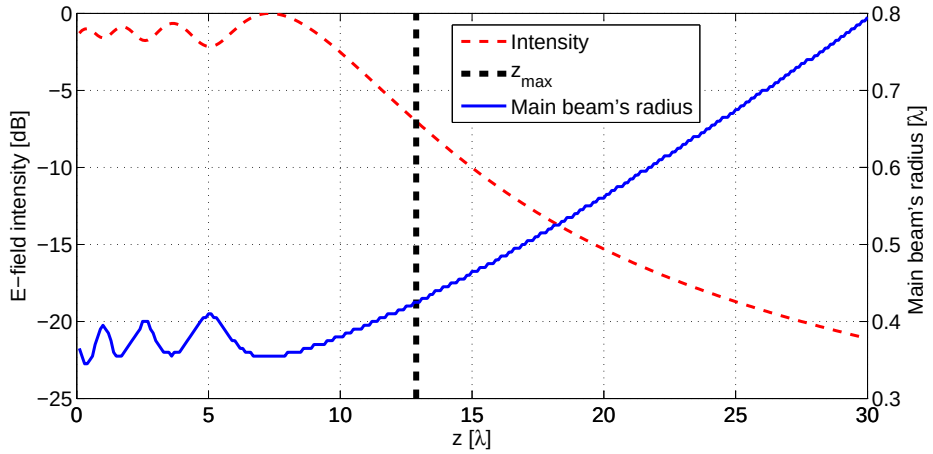

Figure 2.2: The E-field intensity on the axis and the main beam radius of a circular pseudo-Bessel aperture vs. distance from the aperture. The aperture radius $a = 7\lambda$, $k_\rho = 10$.

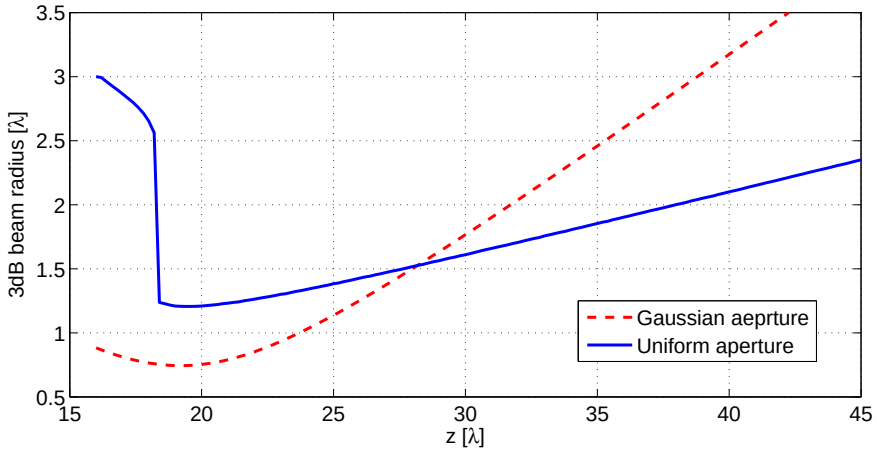

Figure 2.3: Comparison of the 3db beam radii of Gaussian and uniform apertures of identical size.

Another class of infinitely large aperture distributions is the Gaussian aperture [2], where the amplitude distribution of the aperture follows a Gaussian distribution and where a spherical phase distribution controls the location of the beamwaist corresponding to the point where beam is narrowest. The interesting property of Gaussian apertures is that the field distribution at any plane parallel to the aperture remains a Gaussian distribution exhibiting no sidelobes in the near-field. The drawback of a Gaussian aperture is the relatively high rate at which the beam widens after the focus point. This effect is illustrated in Fig. 2.3, where the 3dB beam radius of a uniform field aperture with 5λ radius is compared to a Gaussian aperture with the same 8.7dB radius on the aperture. For the sake of comparison, the focal distances are set to be the same in this figure. This causes the available power to spread over a larger area and, hence, decreases the peak intensity of the field. This decay is even larger in lossy media as it affects the field intensity.

Chapter 3

Near-field Penetration Ability of Antennas in Lossy Media

Antenna far-field characteristics, such as the radiation pattern, directivity, gain, and radiation efficiency are not completely suitable when it comes to near-field applications. As an example, assume a system of two antennas in a sensing system, where one transmits a signal and the other one acts as the receiver and where the received signal is used to extract information on the environment in between both antennas. Generally, it is desirable to maximize the ratio of the received power to the input power in order to increase the signal-to-noise ratio and, hence, to enhance the accuracy of the extracted information. If the antennas were located in the far-field region of each other, assuming a fixed radiation efficiency one could deduce that the ratio of the received power to the input power is increased by an increase in directivity of both antennas; as a rule of thumb, larger sizes of the antennas would lead to higher directivities [1, 22]. But what if the antennas were located close to each other? Does a larger antenna size still lead to a higher power transfer ratio?

3.1 Penetration Ability

Consider the through-sensing system as shown in Fig. 3.1, where two antennas are located opposite to each other on either side of a lossy material. The **total penetration coefficient** p_{totTS} and the **penetration coefficient** p_{TS} for a through-sensing (TS) system are respectively defined as

$$p_{\mathrm{totTS}} = \frac{P_{\mathrm{rec}}}{P_{\mathrm{in}}} \tag{3.1a}$$

$$p_{\mathrm{TS}} = \frac{P_{\mathrm{rec}}}{P_{\mathrm{trans}}} \tag{3.1b}$$

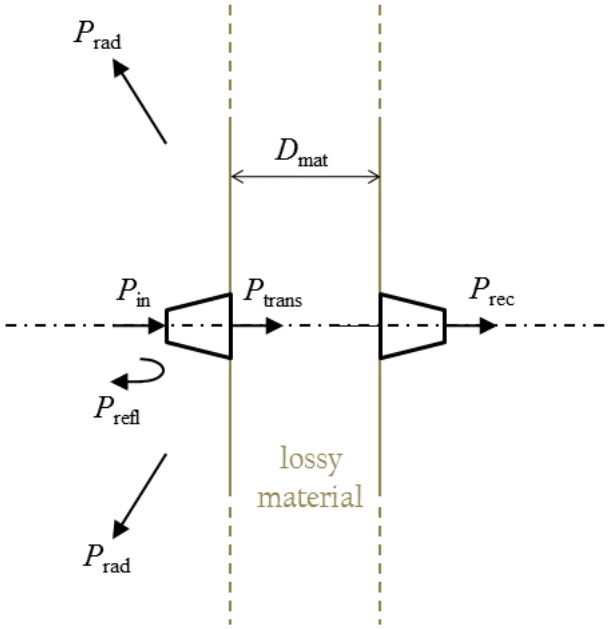

Figure 3.1: Schematic diagram of a through-sensing system.

where P_{rec}, P_{in} and P_{trans} are the received power by the receiving antenna, the input power at the port of transmitting antenna, and the radiated power from the transmitting antenna, respectively. The penetration coefficient and the total penetration coefficient are related to each other through

$$p_{\mathrm{tot\,TS}} = e_{\mathrm{imp}} p_{\mathrm{TS}}, \tag{3.2}$$

where $e_{\mathrm{imp}} = P_{\mathrm{trans}}/P_{\mathrm{in}} = (1-|\Gamma|^2)$ is impedance match efficiency where Γ is the reflection coefficient at the transmitting antenna. The impedance match at the transmitting antenna includes the effect of the near-field surroundings and even the presence of the receiving antenna (sensor). Therefore, the impedance match efficiency is dependent on the environment and the antennas.

When the sensing system is working over a wide frequency band, the total penetration coefficient can be evaluated by frequency domain measurements as

$$p_{\mathrm{tot\,TS}} = \frac{\int_{-\infty}^{\infty} |\tilde{V}_{\mathrm{rec}}(f)|^2 \,\mathrm{d}f}{\int_{-\infty}^{\infty} |\tilde{V}_{\mathrm{in}}(f)|^2 \,\mathrm{d}f} \approx \frac{\int_{f_l}^{f_h} |\tilde{V}_{\mathrm{in}}(f)|^2 |S_{21}(f)|^2 \,\mathrm{d}f}{\int_{f_l}^{f_h} |\tilde{V}_{\mathrm{in}}(f)|^2 \,\mathrm{d}f} \tag{3.3}$$

where f_l and f_h are the lower and higher ends of the operating frequency band of the sensing system, and $\tilde{V}_{\mathrm{rec}}(f)$ and $\tilde{V}_{\mathrm{in}}(f)$ are spectral voltage

signals at the antenna ports. The ports 1 and 2 are connected to the Tx and Rx antennas, respectively. Similarly, we have

$$p_{\mathrm{TS}} = \frac{\int_{f_l}^{f_h} |\tilde{V}_{\mathrm{in}}(f)|^2 |S_{21}(f)|^2 \, \mathrm{d}f}{\int_{f_l}^{f_h} |\tilde{V}_{\mathrm{in}}(f)|^2 (1 - |S_{11}(f)|^2) \, \mathrm{d}f} \tag{3.4}$$

From (3.3) and (3.4), it is clear that the penetration coefficients generally depend on the shape of the transmitted pulse. Assuming that the input signal has a uniform spectral density over the bandwidth $[f_l, f_h]$, (3.3) and (3.4) will reduce to

$$p_{\mathrm{totTS}} = \frac{\int_{f_l}^{f_h} |S_{21}(f)|^2 \, \mathrm{d}f}{f_h - f_l} \tag{3.5a}$$

$$p_{\mathrm{TS}} = \frac{\int_{f_l}^{f_h} |S_{21}(f)|^2 \, \mathrm{d}f}{\int_{f_l}^{f_h} (1 - |S_{11}(f)|^2) \, \mathrm{d}f} \tag{3.5b}$$

3.2 Measurement Results

We will apply the definitions of the penetration coefficient and the total penetration coefficient to three different UWB antennas in order to compare their near-field performance. The three antennas that are examined are the self-grounded Bow-Tie antenna [23,24], Vivaldi antenna [25], and Antipodal

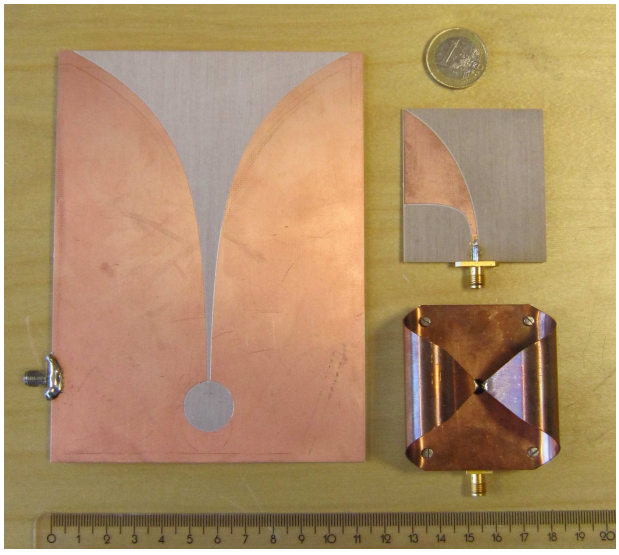

Figure 3.2: Three investigated UWB antennas: Vivaldi (left), Antipodal Vivaldi (top right), and Self-grounded Bow-Tie antenna (bottom right).

Vivaldi antenna [26]. These antennas are shown in Fig. 3.2, where one can compare their sizes.

For the lossy material separating the antennas, blocks of butter with a thickness ranging from 25 mm to 100 mm are used. The choice of butter is due to to the fact that it resembles the permittivity of body fat. The actual average permittivity and loss of butter was measured in the working frequency band using Agilent's 85070E performance probe [27, 28], yielding

$$\epsilon_r = 4.6, \quad \tan\delta = 0.04.$$

During the measurement procedure, a pair of identical antennas are aligned on either side of the blocks of butter with different thicknesses, after which S_{11} and S_{21} were measured by using a network analyzer over the 2GHz to 13.5GHz frequency band. The results are then used to calculate the total penetration and penetration coefficient according to (3.5a) and (3.5b). The results are plotted in Fig. 3.3 and 3.4, respectively. It shows that different antennas perform differently at different depths of interest, e.g., for larger distances, the Vivaldi antenna displays a better performance, whereas it is outperformed by the other two antennas for the closer range.

3.3 Summary and Conclusions

It has been shown that one cannot estimate the penetration ability of different antennas near-field in lossy media by using far-field characteristics of the antenna. Furthermore, the amount of power that each antenna radiates

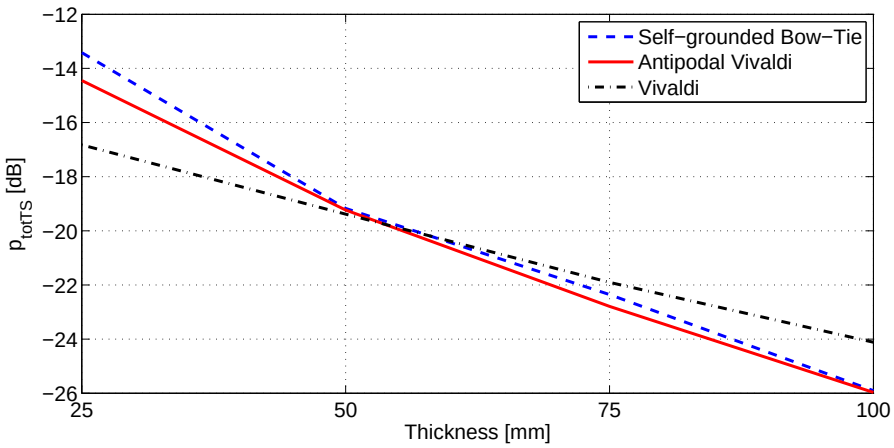

Figure 3.3: The total penetration coefficient of three different antennas vs. the thickness of the lossy medium separating the antennas.

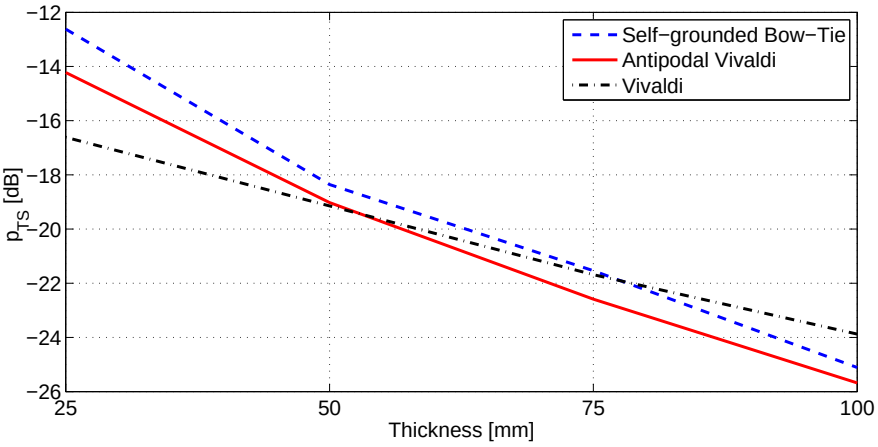

Figure 3.4: The penetration coefficient of three different antennas vs. the thickness of the lossy medium separating the antennas.

in a desired direction in the far- and near-field (i.e. Directivity and Penetration Ability) are not necessarily correlated. The penetration ability is highly dependent on the depth in the lossy medium, the electrical properties of the material itself and the type of the antenna. Paper 1 in Part II of this thesis details this topic further by providing supplementary simulation and measurement results, along with a time domain evaluation of the total penetration coefficient in addition to the frequency domain results.

Based on the results, it is deduced that an optimal antenna aperture size for maximum penetration exists, since the larger size does not lead to higher penetration while a very small size will lead to propagation in various undesired directions. The issue of the optimal aperture size will be further investigated in the next chapter.

Chapter 4

3dB Near-field Beam Radius and Optimal Size of a Uniform Field Aperture

When dealing with focused apertures, the axial pattern has been used as a measure to characterize the antenna near-field focusing capabilities. However, as it has been demonstrated in Fig. 2.1, the axial pattern does not efficiently characterize the antenna focus in the presence of medium losses. Hence, other characterizing parameters are needed in order to investigate the near-field focusing capabilities of antennas the in the presence of medium losses.

4.1 3dB Near-field Beam Radius

The field radiated by a circular uniform field aperture of radius 5λ that is located in the xy-plane at $z = 0$ in brain tissue ($\epsilon_r = 57.5, \sigma = 1.22$ S/m at 1 GHz [29]), is plotted in Fig. 4.1 for two different normalization schemes. In the first plot, the E-field intensity is normalized to the overall maximum and demonstrates a rapid attenuation with distance from the aperture due to losses in the medium, whereas the E-field intensity in the latter is normalized separately at each plane parallel to the aperture. The source current is a y-polarized Huygen's source. As can be observed in this simple illustration, although the field intensity is attenuated heavily with an increase in distance from the aperture, the focus of the available power varies along the axis of the aperture. For example, the uniform aperture in this case, has its narrowest focus around 23λ distance from the aperture. This leads us to the definition and use of the 3dB near-field beam radius.

The 3dB near-field beam radius is defined as the radius of the smallest

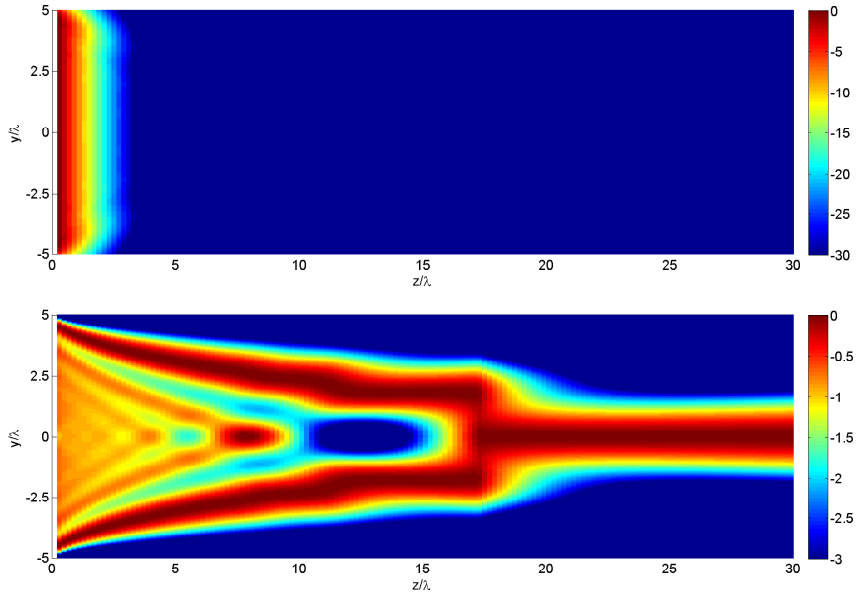

Figure 4.1: The E-plane field intensity of a circular uniform aperture in brain tissue, normalized to the overall maximum (top), and normalized at each plane parallel to the aperture (bottom). The aperture is located at $z = 0$.

circle on each plane parallel to the aperture, which contains all field points where the field strength (intensity of E-field) is higher than -3dB of the strongest strength value in that plane. In other words, all field points outside this 3dB-beam circle have a field strength below -3dB of the strongest value in that plane. The center of the 3dB-beam circle is always on the symmetry axis of the aperture. Note that, although the word "beam" is used in the definition, a beam may not really be formed in the near-field of an antenna. The 3dB near-field beam radius, which is denoted by r_{3dB}, is measured in terms of millimeters or wavelengths, which is different from the 3dB beamwidth used to characterize the far-field radiated beam which is usually measured in degrees. Fig. 4.2 illustrates the definition of the 3dB near-field beam radius for two z-plane cuts carrying different field distributions.

4.2 Aperture Field Calculation

Assume a circular aperture of radius a lying in the xy-plane supporting the electric and magnetic source currents $\boldsymbol{J}$ and $\boldsymbol{M}$, as in Fig. 4.3. The total radiated E-field is given as the sum of contributions from both the electric

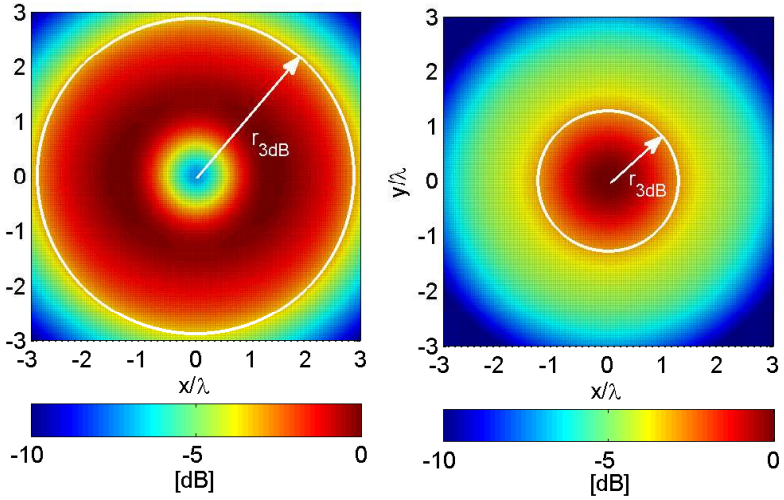

Figure 4.2: Illustrating the definition of the 3dB near-field beam radius through the white circle for two different field distributions, where the maximum on the plane is located off-center (left) and at its center (right) of the 3dB circle.

and magnetic currents [2, pp:145-146], i.e.,

$$\boldsymbol{E}(\boldsymbol{r}) = \boldsymbol{E}_J(\boldsymbol{r}) + \boldsymbol{E}_M(\boldsymbol{r}), \tag{4.1}$$

where

$$\boldsymbol{E}_J(\boldsymbol{r}) = C_k \eta \iint\limits_{S'} \left[\boldsymbol{J} C_{N1} - \left(\boldsymbol{J} \cdot \hat{\boldsymbol{R}} \right) \hat{\boldsymbol{R}} C_{N2} \right] \frac{1}{R} \mathrm{e}^{-jkR} \, \mathrm{d}S' \tag{4.2}$$

$$\boldsymbol{E}_M(\boldsymbol{r}) = C_k \iint\limits_{S'} \left(\boldsymbol{M} \times \hat{\boldsymbol{R}} \right) C_N \frac{1}{R} \mathrm{e}^{-jkR} \, \mathrm{d}S' \tag{4.3}$$

with $\eta = \sqrt{\mu/\epsilon}$ as the wave impedance, $k = 2\pi/\lambda$ as the wavenumber and

$$\mathbf{R} = \mathbf{r} - \mathbf{r}', \quad R = |\mathbf{r} - \mathbf{r}'|, \quad \hat{\mathbf{R}} = \frac{\mathbf{R}}{R}, \quad C_k = \frac{-jk}{4\pi}, \quad C_N = 1 + \frac{1}{jkR},$$
$$C_{N1} = 1 + \frac{1}{jkR} - \frac{1}{(kR)^2}, \quad C_{N2} = 1 + \frac{3}{jkR} - \frac{3}{(kR)^2}.$$

For the discussions in this chapter, we deal with uniform apertures and without losing generality we further assume that the source current is y-polarized, that is,

$$\boldsymbol{J}(\rho') = C\hat{\mathbf{y}}, \quad \rho' \leq a \tag{4.4}$$

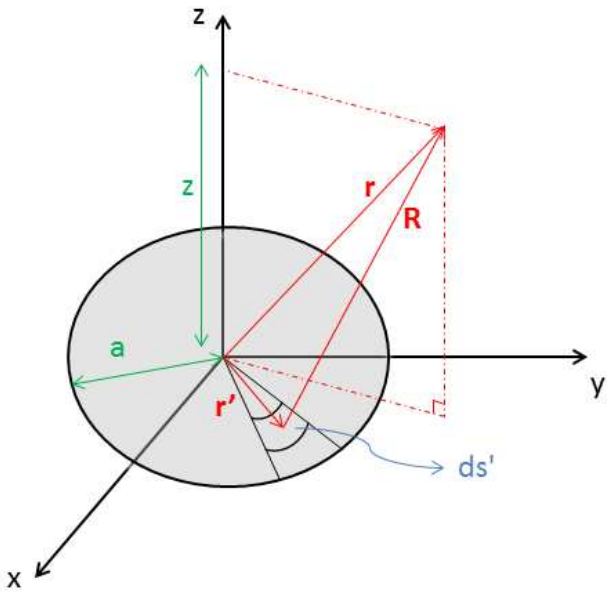

Figure 4.3: A circular aperture in the xy-plane.

for the electric current, and

$$\boldsymbol{M}(\rho') = C\widehat{\mathbf{x}}, \quad \rho' \leq a \tag{4.5}$$

for the magnetic current. Furthermore for the Huygen's source we have

$$\begin{cases} \boldsymbol{J}(\rho') & = C\widehat{\mathbf{y}}, \quad \rho' \leq a \\ \boldsymbol{M}(\rho') & = -C\eta\widehat{\mathbf{x}}), \quad \rho' \leq a \end{cases} \tag{4.6}$$

where C is an arbitrary scalar constant.

4.3 Focal Distance and Optimal Size of Uniform Field Apertures

It has been observed that the 3dB beam radius is independent of the type of the current sources. This independence is demonstrated in Fig. 4.4, which shows the 3dB beam radius along the propagation direction (z-axis) for a uniform aperture field ($a = 5\lambda$) supporting the electric, magnetic or Hyugen's current sources embedded in two different materials (i.e. either free space, or a medium with $\epsilon_r = 10$, $\mu_r = 1$ and $\tan\delta = 0.2$). To understand this independence, we should bear in mind that the 3dB beam radius is defined based on the relative field intensity (compared to its maximum).

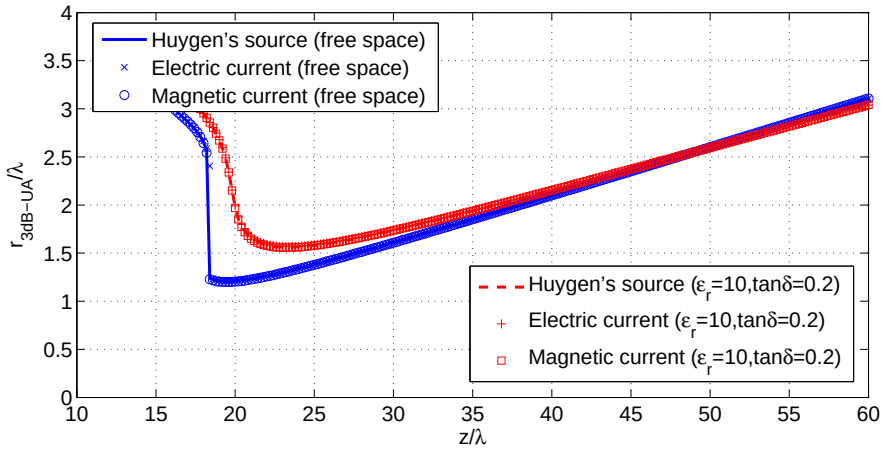

Figure 4.4: Comparison of the beam radius profile generated by different current source types on an aperture of radius $a = 5\lambda$. The blue curves show the free-space case and the red curves show a medium with $\epsilon_r = 10$ and $\tan\delta = 0.2$.

The equality of the beam radius for electric and magnetic currents can be explained through the duality theorem [30, pp:310-312]. The equality of the beam radius for the Huygen's source with the others is explained by the fact that the electromagnetic fields are linear functions of the current sources and superposition can be applied to them. This means implies that we only need to take into account one type of current; the Huygen's source is chosen for this purpose.

If we calculate the 3dB beam radius for different uniform aperture sizes and in different media, it is observed that for any aperture size, there is a certain distance where the beam radius attains its smallest value ($z_{\min}$). Beyond this distance, the beam transforms into a far-field beam and the beam radius increases at a constant rate. In a through-sensing system as shown in Fig. 3.1, the scattering from a foreign object will be the strongest if the object is located at a depth around $z_{\min}$, since that is the depth where the focus size is the smallest. Hence, by knowing the location and the size of the focus for each aperture size in a given media, one can find its optimal size for each application based on the depth of interest. To this end, we have investigated the effect of the medium properties and the size of the aperture on $z_{\min}$, and the beam radius at the focal point $r_{3\text{dBmin}}$. Plots of $z_{\min}$ and $r_{3\text{dBmin}}$ as functions of the aperture radius for five different media are shown in Fig. 4.5. The electrical properties of these media are summarized in Table 4.1. It can be concluded that $z_{\min}$ and $r_{3\text{dBmin}}$ in terms of wavelength (i.e. $z_{\min}/\lambda_{\text{m}}$ and $r_{3\text{dBmin}}/\lambda_{\text{m}}$, where λ_{m} is the wavelength

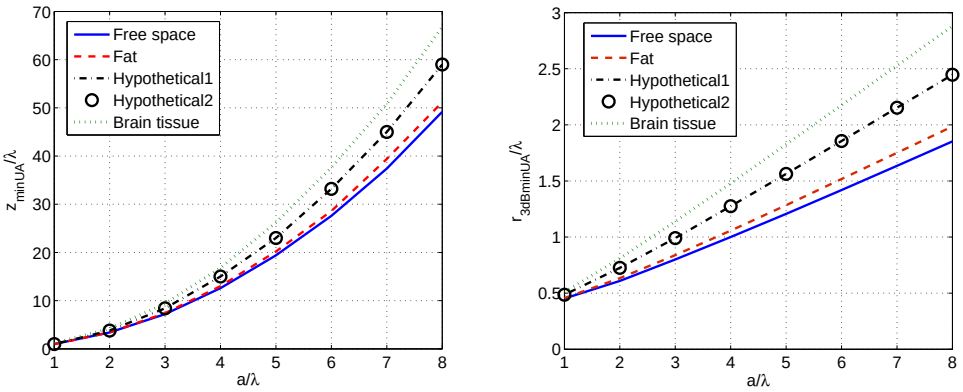

Figure 4.5: Location and size of uniform aperture's focus vs. aperture radius for different media.

Table 4.1: Electric properties of five of the investigated media.

Medium	ϵ_r	$\tan\delta$
Free space	1	0
Fat	10	0.04
Hypothetical 1	10	0.2
Hypothetical 2	5	0.2
Brain tissue	57.5	0.38

in medium) are independent of the medium permittivity and are affected only by loss. Furthermore it is observed that $z_{\min}/\lambda_{\mathrm{m}}$ and $r_{3\mathrm{dBmin}}/\lambda_{\mathrm{m}}$ both increase with an increase in the medium losses. Based on these results and those done for other investigated media, we can derive empirical formulae for $z_{\min}/\lambda_{\mathrm{m}}$ and $r_{3\mathrm{dBmin}}/\lambda_{\mathrm{m}}$ pertaining to a uniform field aperture as a function of the medium loss and aperture radius as:

$$\frac{r_{3\mathrm{dBminUA}}}{\lambda_{\mathrm{m}}} = (0.2067 - 0.1985\tan\delta) + (0.2060 + 0.3650\tan\delta)\left(\frac{a}{\lambda_{\mathrm{m}}}\right) \tag{4.7a}$$

$$\frac{z_{\mathrm{minUA}}}{\lambda_{\mathrm{m}}} = \left(0.3101 - 1.6993\tan\delta + 3.2400\tan^2\delta\right) - \left(0.0102 - 0.2552\tan\delta + 0.6960\tan^2\delta\right)\left(\frac{a}{\lambda_{\mathrm{m}}}\right) + \left(0.7632 + 0.8137\tan\delta - 0.2149\tan^2\delta\right)\left(\frac{a}{\lambda_{\mathrm{m}}}\right)^2 \tag{4.7b}$$

4.4 Summary and Conclusion

It has been shown that the axial pattern cannot be used in the presence of medium losses, since forelobes and aftlobes do not appear due to the field attenuation. Instead, the 3dB near-field beam radius is introduced and used to investigate the focusing properties of uniform apertures. The 3dB near-field beam radius has shown to be independent of the type of current source and can be defined for any shape of the aperture, which makes it a general parameter applicable to various types of apertures. More details and results are presented in the Papers 2 and 3 in Part II of this thesis.

It is further suggested that by choosing a suitable size of the antenna aperture, depending on medium loss and depth of interest, one can enhance the amount of scattered power from a foreign object in a through-sensing system. Empirical formulae for the focal distance and the corresponding beam radius at the focal plane are provided, which are used in determining the optimal size of the uniform aperture. The optimal size of the uniform aperture for the detection of foreign objects in lossy media, as well as the effect of correctly chosen aperture size on the scattered power from objects is investigated and presented in Paper 3 with an idealized test setup.

Chapter 5

Optimal Aperture Fields For Maximum Power Transfer in Lossy Media

In the previous chapter, we introduced and discussed the 3dB near-field beam radius and its relation to the antenna focus in the near-field for the case of lossy media and subsequently used it to find an optimal size of a uniform aperture for the detection of foreign objects. In the present chapter we will take another approach to the synthesis of the optimal aperture field problem, that is, to numerically find the optimal aperture distribution that maximizes the power coupling between two antennas separated by a lossy medium, given a fixed receiver size and antenna separation distance. The applications for such optimal apertures include, but are not limited to wireless power transfer to implants and in-body communication with these implants, where the receiver is typically very small. It is argued that maximizing the power coupling between two antennas will enhance the detection probability of foreign objects in sensing applications, since the disturbance in the presence of any foreign object is likely to be maximized as well.

5.1 Problem Setup and Power Transfer Ratio

The problem setup is illustrated in Fig. 5.1. Two antennas are separated by a lossy medium with a complex-valued characteristic impedance η. The objective is to find an electric ($\boldsymbol{J}$) and magnetic ($\boldsymbol{M}$) current distribution that maximizes the ratio of the received power to the total input power. Since the medium is lossy, the effect of the backscattered field at the receiving side on the transmitting side can be neglected. Hence, one can assume

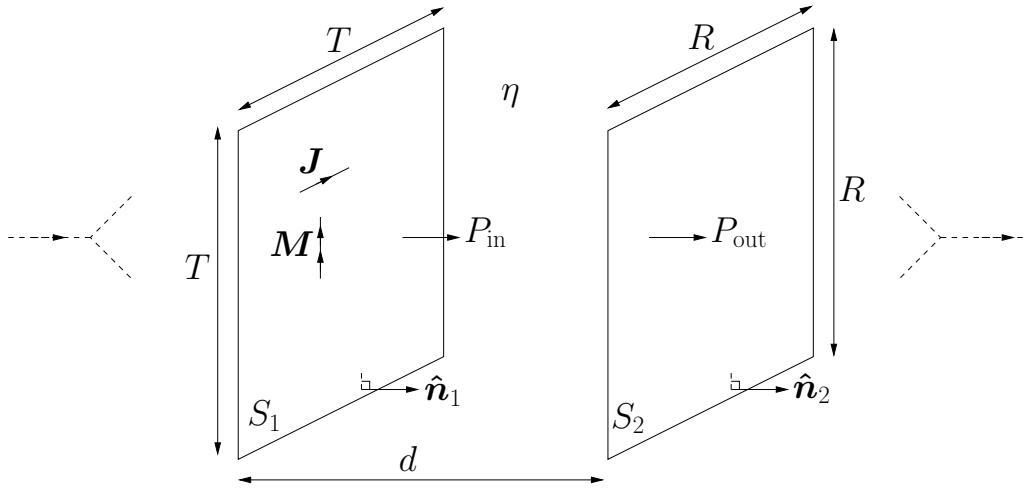

Figure 5.1: Problem setup including a transmitting and an ideally receiving aperture antenna.

that the source currents $\boldsymbol{J}$ and $\boldsymbol{M}$ radiate in a homogenous medium with characteristic impedance η. The total received power P_{out} is given by

$$P_{\text{out}} = \frac{1}{2}\mathfrak{Re}\left\{\int_{S_2} [\boldsymbol{E}(\boldsymbol{J},\boldsymbol{M}) \times \boldsymbol{H}^*(\boldsymbol{J},\boldsymbol{M})] \cdot \hat{\boldsymbol{n}}_2 \,\mathrm{d}S\right\}. \tag{5.1}$$

Similarly, the supplied power P_{in} is given by

$$P_{\text{in}} = \frac{1}{2}\mathfrak{Re}\left\{\int_{S_1} [\boldsymbol{E}(\boldsymbol{J},\boldsymbol{M}) \times \boldsymbol{H}^*(\boldsymbol{J},\boldsymbol{M})] \cdot \hat{\boldsymbol{n}}_1 \,\mathrm{d}S\right\}. \tag{5.2}$$

Next if we expand $\boldsymbol{J}$ and $\boldsymbol{M}$ in terms of N basis functions as

$$\boldsymbol{J} = \sum_{n=1}^{N} j_n \boldsymbol{f}_n(\boldsymbol{r}), \quad \boldsymbol{M} = \sum_{m=1}^{N} m_m \boldsymbol{g}_m(\boldsymbol{r}) \tag{5.3}$$

and substitute (5.3) in (5.1) and (5.2), the supplied and received powers can be written after some manipulations as

$$P_{\text{out}} = \frac{1}{2}\mathfrak{Re}\{\mathbf{w}^H \mathbf{P}_{\text{out}} \mathbf{w}\} \tag{5.4a}$$

$$P_{\text{in}} = \frac{1}{2}\mathfrak{Re}\{\mathbf{w}^H \mathbf{P}_{\text{in}} \mathbf{w}\} \tag{5.4b}$$

where $\mathbf{P}_{\text{in}}$ and $\mathbf{P}_{\text{out}}$ are system matrices for the input and output powers, and where $\mathbf{w}$ is the vector containing the unknown weights j_n and m_m of the basis functions, i.e.,

$$\mathbf{w} = \begin{bmatrix} \mathbf{j} \\ \mathbf{m} \end{bmatrix}.$$

The derivation of $\mathbf{P}_{\text{in}}$ and $\mathbf{P}_{\text{out}}$ in (5.4) is explained in detail in Paper 4 of Part II and is therefore omitted in this chapter to avoid repetition. The objective is to maximize the ratio of the received power to the supplied input power, or power transfer ratio (P_{tr}), which can be written as

$$P_{\text{tr}} = \frac{P_{\text{out}}}{P_{\text{in}}} = \frac{\mathfrak{Re}\left\{\mathbf{w}^H \mathbf{P}_{\text{out}} \mathbf{w}\right\}}{\mathfrak{Re}\left\{\mathbf{w}^H \mathbf{P}_{\text{in}} \mathbf{w}\right\}} = \frac{\mathbf{w}^H [\mathbf{P}_{\text{out}} + \mathbf{P}_{\text{out}}^H] \mathbf{w}}{\mathbf{w}^H [\mathbf{P}_{\text{in}} + \mathbf{P}_{\text{in}}^H] \mathbf{w}} \tag{5.5}$$

5.2 Maximization

Since w_i are complex valued weights, that is, $w_i = w_i' + jw_i''$ for $i = 1, 2, \ldots, 2N$, to find the maximum of $P_{\text{tr}}\left(\mathbf{w}, \mathbf{w}^H\right)$, we require that both

$$\frac{\partial P_{\text{tr}}}{\partial w_i'} = 0 \quad \text{and} \quad \frac{\partial P_{\text{tr}}}{\partial w_i''} = 0 \tag{5.6}$$

which on account of the chain rule for differentiation, are written as

$$\frac{\partial P_{\text{tr}}}{\partial w_i'} = \frac{\partial P_{\text{tr}}}{\partial w_i}\frac{\partial w_i}{\partial w_i'} + \frac{\partial P_{\text{tr}}}{\partial w_i^*}\frac{\partial w_i^*}{\partial w_i'} = \frac{\partial P_{\text{tr}}}{\partial w_i} + \frac{\partial P_{\text{tr}}}{\partial w_i^*} = 0 \tag{5.7a}$$

$$\frac{\partial P_{\text{tr}}}{\partial w_i''} = \frac{\partial P_{\text{tr}}}{\partial w_i}\frac{\partial w_i}{\partial w_i''} + \frac{\partial P_{\text{tr}}}{\partial w_i^*}\frac{\partial w_i^*}{\partial w_i''} = j\left(\frac{\partial P_{\text{tr}}}{\partial w_i} - \frac{\partial P_{\text{tr}}}{\partial w_i^*}\right) = 0 \tag{5.7b}$$

which implies, (5.6) is satisfied, if and only if,

$$\frac{\partial P_{\text{tr}}}{\partial w_i} = 0 \quad \text{and} \quad \frac{\partial P_{\text{tr}}}{\partial w_i^*} = 0. \tag{5.8}$$

By setting $\mathbf{A} = \mathbf{P}_{\text{out}} + \mathbf{P}_{\text{out}}^H$ and $\mathbf{B} = \mathbf{P}_{\text{in}} + \mathbf{P}_{\text{in}}^H$ in (5.5), we can write P_{tr} as

$$P_{\text{tr}} = \frac{N}{D} = \frac{\sum_n^N \sum_m^N w_n^* A_{nm} w_m}{\sum_n^N \sum_m^N w_n^* B_{nm} w_m} \tag{5.9}$$

substituting (5.9) in (5.8) gives

$$\frac{\partial P_{\text{tr}}}{\partial w_i} = \frac{1}{D^2}\left[D\sum_n^N w_n^* A_{ni} - N\sum_n^N w_n^* B_{ni}\right] = 0, \quad \forall i \tag{5.10a}$$

$$\frac{\partial P_{\text{tr}}}{\partial w_i^*} = \frac{1}{D^2}\left[D\sum_m^N A_{im} w_m - N\sum_m^N B_{im} w_m\right] = 0, \quad \forall i \tag{5.10b}$$

now, by assuming $D \neq 0$, which means that the supplied power is not zero, equation (5.10b) can be written as

$$\mathbf{A}\mathbf{w} = P_{\text{tr}}\mathbf{B}\mathbf{w} \tag{5.11}$$

and since both $\mathbf{A}$ and $\mathbf{B}$ are Hermitian matrices, (5.10a) will also reduce to (5.11). This is a generalized eigenvalue problem and the largest positive value of P_{tr} is equal to the largest eigenvalue with the corresponding principal eigenvector $\mathbf{w} = \mathbf{w}_{\text{opt}}$ [31, pp:189-193]. For any given geometry and medium properties, $\mathbf{P}_{\text{in}}$ and $\mathbf{P}_{\text{out}}$ can be computed and $\mathbf{w}_{\text{opt}}$ can be found.

5.3 Results

The resulting optimal aperture field distributions are observed to have the following general properties:

- The field has rotational symmetry around the axis of the aperture, which is to be expected from the geometry of the problem.
- The phase of the field on the edge of the aperture is leading relative to the center of the aperture resulting in a constructive interference of wavefronts originating from different parts of the transmitting aperture close to the center of the receiver aperture.
- The field amplitude is tapered with the highest amplitude in the aperture center. Since the propagation distance from the aperture edge to the receiver is longer compared to its center, the field attenuation is higher. Hence, the power of the optimally synthesized aperture field is less concentrated close to the edge.
- The electric and magnetic currents appear to be closely related through

  $$\boldsymbol{M}(\boldsymbol{r}) = \eta^* \hat{\boldsymbol{n}}_1 \times \boldsymbol{J}(\boldsymbol{r}).$$

  This means that the optimal aperture field distribution requires that the electric and magnetic currents contribute by the same amount to the total field.

The normalized magnitude and phase of $\boldsymbol{J}$ for different transmitter aperture sizes are plotted in Fig. 5.2, where the assumed receiver aperture size is $1\lambda \times 1\lambda$ and where the apertures are separated by 4λ in muscule tissue ($\epsilon_r = 57, \sigma = 1.2$ S/m at 1 GHz [32]). Note that the value of x along the horizontal axis in this figure is normalized to its largest value for each transmitting aperture size. This means that the $[-1, 1]$ span on the horizontal axis covers the whole length of the aperture and thus shows different lengths for different aperture sizes. It is observed that as the aperture size becomes larger, the tapering in amplitude and phase also increases.

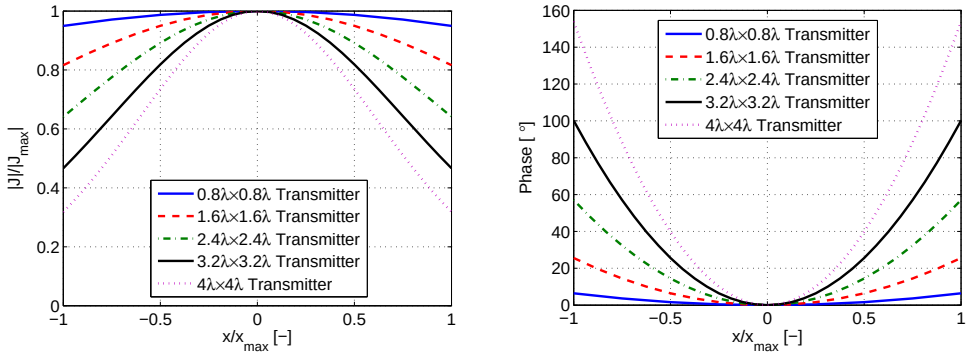

Figure 5.2: Normalized amplitude (left) and phase in degrees (right) of the optimal electric current distribution on the transmitter aperture. The receiver is $1\lambda \times 1\lambda$ located 4λ away from the transmitter.

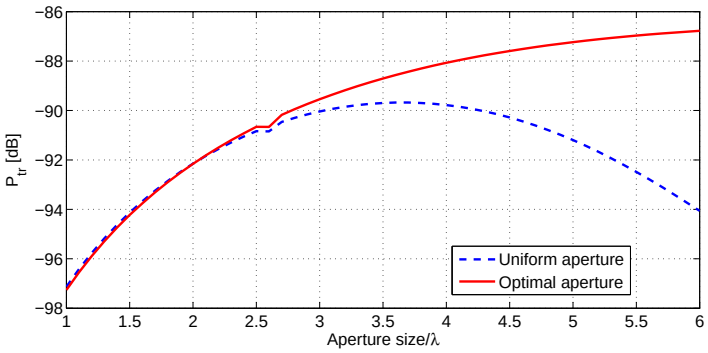

Figure 5.3: Comparison of the power transfer ratios of the optimal and uniform apertures vs. the aperture size.

The power transfer ratios of the optimal apertures of sizes $\lambda \times \lambda$ to $6\lambda \times 6\lambda$ are compared to those obtained for the uniform apertures of the same size. The results are shown in Fig. 5.3 assuming a $\lambda \times \lambda$ receiver aperture and a 8λ distance between the two apertures embedded in muscle tissue. A uniform aperture is chosen as a reference for the comparisons since it is the aperture distribution which is known to provide the highest directivity in the far-field. It can be observed that the P_{tr} for a uniform aperture field decreases when the aperture exceeds a certain size due to the spreading of the power over a larger area in the near-field. However, the optimal aperture can maintain the level of the power transfer ratio even for larger sizes. It should be noted that the P_{tr} value of the optimal aperture will saturate beyond a certain size due to the attenuation of the field as a result of which it cannot increase further. The saturation size depends on the size of the receiving aperture, the distance between the transmitting and

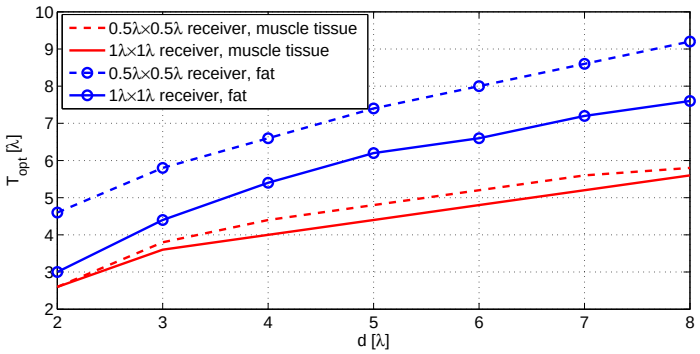

Figure 5.4: T_{opt} vs. distance for different receiver sizes in two media.

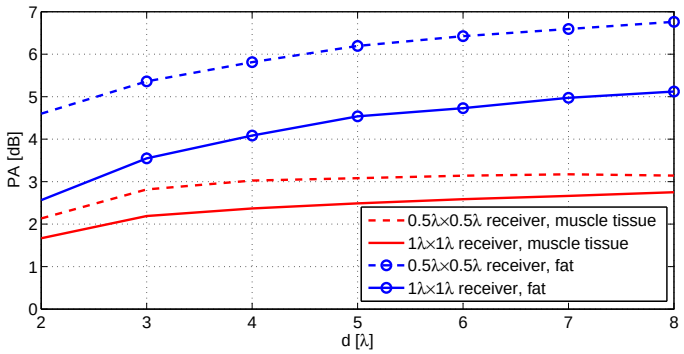

Figure 5.5: PA vs. distance for different receiver sizes in two media.

receiving apertures, and the loss in the medium. This saturation further implies that there is an optimal size for the optimal aperture filed beyond which the increase in P_{tr} is insignificant.

Plots of the optimal aperture size for the optimal aperture field (T_{opt})and the amount of P_{tr} advantage (PA) relative to the P_{tr} of the best uniform aperture vs. the distance between the two apertures, can be generated for different receiver aperture sizes and for different media. These plots are useful in system design phases where the receiver size and distance are already fixed and where the medium properties are known. In such cases, we can readily determine the optimal aperture size in combination with an optimal aperture field distribution providing the maximum achievable improvement in power transfer ratio. Figures 5.4 and 5.5 show T_{opt} and PA vs. distance (d) for different receiver aperture sizes in muscle tissue and fat ($\epsilon_r = 4.6, \sigma = 0.02$ S/m at 1 GHz). It is observed that the increase in loss calls for smaller optimal apertures. However, it should be noted that the amount of P_{tr} advantage over a uniform aperture will also decrease with an increase in medium loss.

5.4 Summary and Conclusions

A novel numerical optimization method to determine the optimal aperture field distribution for maximum power transfer between two idealized aperture antennas through a lossy medium is presented. The optimal aperture field can be used as a reference field in the system design of different applications dealing with the problems of wireless power transfer to implants, near-field communications with implants, and detection of foreign objects in lossy media. The effect of the size of the apertures and the separation distance between the two antennas have been investigated for different dielectric properties of the medium. More details on the optimization procedure and its results are presented in Paper 4 in Part II of the thesis.

Chapter 6

Contributions and Future Work

Research into near-field microwave systems, for sensing and detection, wireless power transfer, and near-field communication applications, have increased in recent years. An essential part of these microwave systems is the antenna which has to be designed in order to meet specific near-field criteria. Furthermore, and as opposed to the far-field, near-field antenna characteristics and design criteria are not as well defined and established, in particular when the medium surrounding the antenna is lossy, as is the case in many of the aforementioned near-field microwave applications.

The *penetration ability* is introduced in Chapter 3 and Paper 1 as a parameter to characterize antennas in the near-field, which is particularly useful when the medium is lossy. For instance, by investigating the penetration ability, it has been shown that the far-field characteristics, such as directivity, cannot be used to estimate the amount of power an antenna radiates in a given direction in the near-field.

In Chapter 4, and both the Papers 2 and 3, the *3dB near-field beam radius* is introduced and used as a parameter to characterize the antenna's near-field focusing ability in lossy media, since the commonly studied axial pattern is no longer an adequate quantity when medium loss is present. The 3dB near-field beam radius has been exploited to determine the optimal size of a uniform aperture field for the near-field detection of foreign objects in lossy media.

A generic numerical method for determining the optimal aperture field distribution that maximizes the near-field power transfer through lossy media is developed and described in Chapter 5, as well as in Paper 4. The optimal apertures, which are determined by applying array signal processing techniques to aperture field modes, can be used to: (i) explore fundamental limits of near-field antenna systems; (ii) derive a reference field distribution that can be used to design transmitting and receiving antennas with the aid of aperture field matching techniques; (iii) develop optimal design curves,

thereby alleviating the initial design problem. In this chapter specifically, the performance of the optimal aperture fields are compared to the uniform one, the latter of which is known to provide the highest far-field directivity, and practical design curves for the estimation of the achievable advantage in terms of the power transfer ratio for different receiver sizes and media are examined and presented.

6.1 Future Work

Since the numerical method that is presented in Chapter 5 is generic and flexible, it can be applied to apertures of different sizes and shapes including those that are not planar. Since the analysis is currently limited to homogenous media – due to the employed Green's function – one of the aspects for further development is to use algorithms such as G1DMULT [33] in order to extend the modeling capabilities to multi-layered symmetric geometries like spherical or cylindrical structures. Another interesting possibility is to import the optimal source reference field distribution into a commercial EM solver, introduce a foreign object in the medium, and estimate the detection probability. In this respect, the array-signal-processing-based method, as proposed in Chapter 5 and Paper 4, forms an excellent basis to further examine and develop sensitive detection methods, including those that can decide whether a tissue is cancerous or not.

The present work explores some of the fundamental limits of transferring power in lossy media and provides initial design curves, however, the final objective in the realization process is to actually generate an aperture field that is as close as possible to the optimal one. Hence, another future research direction is to design and realize a detection system employing optimal field-matching transmitting and receiving antennas.

References

[1] C. A. Balanis, *Antenna Theory. Analysis And Design.* New Jersey: John Wiley and Sons, Inc., 2005.

[2] P.-S. Kildal, *Foundations of antennas: A unified approach.* Studentlitteratur, 2000.

[3] K. Rosengren and P.-S. Kildal, "Radiation efficiency, correlation, diversity gain and capacity of six monopole antenna array for a MIMO system: Theory, simulation and measurement in reverberation chamber," *Proceedings IEE, Microwaves Antennas and Propagation*, vol. 152, no. 1, pp. 7–16, 2005.

[4] X. Li, E. Bond, B. Van Veen, and S. Hagness, "An overview of ultra-wideband microwave imaging via space-time beamforming for early-stage breast-cancer detection," *IEEE Antennas and Propagation Magazine*, vol. 47, no. 1, pp. 19–34, 2005.

[5] Y. Yu, J. Yang, T. McKelvey, and B. Stoew, "A compact UWB indoor and through-wall radar with precise ranging and tracking," *International Journal of Antennas and Propagation*, vol. 2012, 2012.

[6] S. Fayazi, J. Yang, and H. Lui, "UWB SAR imaging of near-field object for industrial process applications," in *7th European Conference on Antennas and Propagation, (EuCAP 2013)*, Gothenburg, Sweden, 8-12 April 2013.

[7] X. Zeng, A. Fhager, P. Linner, M. Persson, and H. Zirath, "Experimental investigation of the accuracy of an ultrawideband time-domain microwave-tomographic system," *Instrumentation and Measurement, IEEE Transactions on*, vol. 60, no. 12, pp. 3939–3949, 2011.

[8] K. Sanghoek, J. Ho, and A. Poon, "Wireless power transfer to miniature implants: Transmitter optimization," *IEEE Transactions on Antennas and Propagation*, vol. 60, no. 10, pp. 4838–4845, 2012.

[9] J. W. Sherman, "Properties of focused apertures in the fresnel region," *IRE Transactions on Antennas and Propagation*, vol. 10, no. 31, pp. 399–408, July 1962.

[10] R. C. Hansen, "Focal region characterisitics of focused array antennas," *IEEE Transactions on Antennas and Propagation*, vol. AP-33, no. 12, pp. 1328–1337, December 1985.

[11] W. J. Graham, "Analysis and synthesis of axial field patterns of focused apertures," *IEEE Transactions on Antennas and Propagation*, vol. 31, no. 4, pp. 665–668, July 1983.

[12] S. Karimkashi and A. Kishk, "Focused microstrip array antenna using a dolph-chebyshev near-field design," *IEEE Transactions on Antennas and Propagation*, vol. 57, no. 12, pp. 3813–3820, December 2009.

[13] ——, "Focusing properties of fresnel zone plate lens antennas in the near-field region," *IEEE Transactions on Antennas and Propagation*, vol. 59, no. 5, pp. 1481–1487, May 2011.

[14] A. F. Kay, "Near-field gain of aperture antennas," *IRE Transactions on Antennas and Propagation*, vol. 8, no. 6, pp. 586–593, November 1960.

[15] G. V. Borgiotti, "Maximum power transfer between two planar apertures in the fresnel zone," *IEEE Transactions on Antennas and Propagation*, vol. 14, no. 2, pp. 158–163, March 1966.

[16] J. Durnin, "Exact solutions for nondiffracting beams. I. the scalar theory," *Journal of Optical Society of America A*, vol. 4, no. 4, pp. 651–654, 1987.

[17] J. Durnin, J. Miceli, and J. H. Eberly, "Diffraction-free beams," *Physical Review Letters*, vol. 58, no. 15, pp. 1499–1501, April 1987.

[18] J. Durnin and J. Miceli, "Comparison of bessel and gaussian beams," *Optics Letters*, vol. 13, no. 2, pp. 79–80, February 1988.

[19] P. Lemaitre-Auger, S. Abielmona, and C. Caloz, "Generation of bessel beams by two-dimensional antenna arrays using sub-sampled distributions," *IEEE Transactions on Antennas and Propagation*, vol. 61, no. 4, pp. 1838–1849, 2013.

[20] M. A. Salem, A. H. Kamel, and E. Niver, "Microwave bessel beams generation using guided modes," *IEEE Transactions on Antennas and Propagation*, vol. 59, no. 6, pp. 2241–2247, 2011.

[21] M. Ettorre and A. Grbic, "Generation of propagating bessel beams using leaky-wave modes," *IEEE Transactions on Antennas and Propagation*, vol. 60, no. 8, pp. 3605–3613, 2012.

[22] J. D. Kraus and R. J. Marhefka, *Antennas For All Applications*. McGraw-Hill Education, 2002.

[23] J. Yang and A. Kishk, "The self-grounded Bow-Tie antenna," in *IEEE AP-S International Symposium on Antennas and Propagation*, Spokane, Washington, July 2011.

[24] ——, "A novel low-profile compact directional ultra-wideband antenna: the Self-Grounded Bow-Tie antenna," *IEEE Transactions on Antennas and Propagation*, vol. 60, no. 3, pp. 1214–1220, 2012.

[25] P. J. Gibson, "The vivaldi aerial," *Proceedings of the 9th European Microwave Conference*, pp. 101–105, 1979.

[26] E. Gazit, "Improved design of the vivaldi antenna," in *Proceedings of IEE, Microwaves Antennas and Propagation*, April 1988, pp. 89–92.

[27] "Technical overview, agilent 85070e dielectric probe kit 200 MHz to 50 GHz," Agilent Technologies, Inc., May 9 2003.

[28] "Technical overview, agilent 85071e materials measurement software," Agilent Technologies, Inc., November 6 2003.

[29] G. Schmid, G. Neubauer, and P. Mazal, "Dielectric properties of human brain tissue measured less than 10 h postmortem at frequencies from 800 to 2450 mhz," *Bioelectromagnetics*, vol. 24, no. 6, pp. 423–430, 2003.

[30] C. A. Balanis, *Advanced Engineering Electromagnetics*. New York: John Wiley and Sons, Inc., 1989.

[31] R. F. Harrington, *Field Computation by Moment Methods*. New York: The Macmillan Company, 1968.

[32] S. Gabriel, R. Lau, and C. Gabriel, "The dielectric properties of biological tissues: III. Parametric models for the dielectric spectrum of tissues," *Physics in medicine and biology*, vol. 41, p. 2271, 1996.

[33] P.-S. Kildal, Z. Sipus, and M. Johansson, "G1DMULT–a numerical algorithm for computing green's functions," in *ACES Symposium Monterey, CA*, 1997, pp. 1242–1249.